From VO_2 to V_2O_3: The metal-insulator transition of the Magnéli phase V_6O_{11}

U. Schwingenschlögl(*), V. Eyert and U. Eckern
Institut für Physik, Universität Augsburg - 86135 Augsburg, Germany

PACS. 71.20.-b – Band structure of crystalline solids.
PACS. 71.30.+h – Metal-insulator transitions.
PACS. 72.15.Nj – Collective modes.

Abstract. – The metal-insulator transition (MIT) of V_6O_{11} is studied by means of electronic structure calculations using the augmented spherical wave method. The calculations are based on density functional theory and the local density approximation. Changes of the electronic structure at the MIT are discussed in relation to the structural transformations occurring simultaneously. The analysis is based on a unified point of view of the crystal structures of V_6O_{11}, VO_2, and V_2O_3. This allows to group the electronic bands into states behaving similarly to the dioxide or the sesquioxide. While the sesquioxide-like V $3d_{yz}$ states show rather weak changes on entering the low-temperature structure, some of the dioxide-like V $3d_{x^2-y^2}$ states display splittings and shifts similar to those known from VO_2. The MIT of V_6O_{11} arises as a combination of changes appearing in both of these compounds. Our results shed new light onto the role of particular electronic states for the MIT of V_2O_3.

The binary oxides of vanadium have been attracting considerable interest for many years. This is due to metal-insulator transitions (MIT) displayed by the majority of these compounds, in particular their sensitivity to both electronic correlations and electron-phonon coupling. The delicate interplay of both mechanisms prevents a straightforward understanding of the transitions. As a consequence, the origins of the transitions are still a matter of dispute. This holds especially for the prototypical compounds VO_2 and V_2O_3 [1–3].

The MIT of VO_2 at 340 K is accompanied by a structural transformation from the rutile structure to a monoclinic structure. While both electron-lattice interaction and electronic correlations have been proposed as the origin of the transition [1, 4, 5], recent electronic structure calculations for VO_2 gave strong hints at a Peierls instability of the one-dimensional $d_\parallel$ ($d_{x^2-y^2}$) band in an embedding background of the remaining V $3d$ t_{2g} states [5, 6]. This scenario was supported by studies of the neighbouring compounds MoO_2 and NbO_2 [7, 8]. Yet, since calculations based on the local density approximation (LDA) just miss the insulating gap of low-temperature VO_2, electronic correlations are also expected to be of some relevance.

At a temperature of 168 K and ambient pressure, stoichiometric V_2O_3 experiences a transition from a paramagnetic metallic (PM) phase to an antiferromagnetic insulating (AFI) phase.

(*) E-mail: Udo.Schwingenschloegl@physik.uni-augsburg.de

At the same time, the crystal structure transforms from the corundum to a monoclinic structure. In contrast, on doping with only small amounts of Al or Cr, V_2O_3 enters a paramagnetic insulating (PI) phase without change of the crystal symmetry. Yet, recent EXAFS experiments gave evidence of local crystal-structure distortions in the PI phase, which only in the monoclinic AFI phase display long-range order [9]. The metal-insulator transitions of V_2O_3 are generally regarded as classical examples of a Mott-Hubbard transition [10]. LDA calculations performed for all three phases showed only a minor response of the electronic structures to the crystal parameter changes. The slight narrowing of the characteristic a_{1g} bands in the insulating phases formed the basis for a successful description of the PM-PI transition in a recent study, where LDA calculations were combined with dynamical mean-field theory (DMFT) [11]. This approach, called LDA+DMFT, is especially suited for a realistic modelling of strongly interacting electron systems. The strong influence of electronic correlations has also been demonstrated by LDA+U calculations for the AFI phase [12].

A more comprehensive understanding of both compounds calls for deeper insight into the role of electronic correlations and electron-lattice interaction on going from VO_2 to V_2O_3. In particular, we are interested in the electronic states which are involved in the MIT. In the present paper we address these issues by discussing the results of electronic structure calculations for the Magnéli phase V_6O_{11}. The Magnéli phases of vanadium form a homologous series V_nO_{2n-1} ($3 \leq n \leq 9$) and are particularly suited for studying the differences in crystal structures and electronic properties between the end members VO_2 ($n \to \infty$) and V_2O_3 ($n = 2$). Being part of a broad investigation of the Magnéli phases, our work is the first *ab initio* study of these compounds at all. Relating the different local environments of the vanadium atoms in V_6O_{11} to the electronic properties, we are able to obtain deeper insight into the crossover from the dioxide to the sesquioxide. In particular, we find that the changes of the $d_{x^2-y^2}$ states along the series account for most of the differences.

As the general formula $V_nO_{2n-1} = V_2O_3 + (n-2)VO_2$ suggests, the crystal structures of the Magnéli phases are usually viewed as rutile-type slabs of infinite extension, which are separated by shear planes with a corundum-like atomic arrangement [2, 13, 14]. While in the rutile-type regions the characteristic VO_6 octahedra are coupled via edges, the shear planes have face-sharing octahedra as in the corundum structure.

For a deeper understanding of the electronic properties of all Magnéli phases we have developed a different representation of the crystal structures. It starts out from the regular 3D network of oxygen octahedra, which, apart from a slightly different buckling, is similar for all members including VO_2 and V_2O_3. Differences between the compounds V_nO_{2n-1} arise from the filling of the octahedra with vanadium atoms. Filled octahedra form chains of length n parallel to the pseudo-rutile axis c_{prut}, followed by $n-1$ empty sites. In particular, in VO_2 these chains have infinite length. For V_6O_{11} the situation is sketched in fig. 1, which shows a projection of an O–V–O sandwich-like slab cut out of the crystal structure. In this projection, oxygen octahedra appear as a regular hexagonal network. Both this network and the vanadium chains of length 6 can be identified in the left panel of fig. 1. Perpendicular to the projection, along a_{prut}, vanadium and oxygen layers alternate. Two different types of vanadium layers are distinguished, which comprise vanadium atoms V1, V3, V5, and V2, V4, V6, respectively. Within the vanadium sublattice these layers alternate along a_{prut}. However, vanadium chains in neighbouring vanadium layers are shifted parallel to c_{prut}, so that atoms V1 and V2 are found on top of each other. This situation is sketched on the right panel of fig. 1. The relative shifts of the vanadium chains give rise to different arrangements of the VO_6 octahedra. While octahedra neighbouring along a_{prut} or b_{prut} share faces, coupling between metal atoms along all other directions within the layers is via octahedral edges. Whereas the atomic arrangements near the ends of the chains are similar to those in V_2O_3, coordination

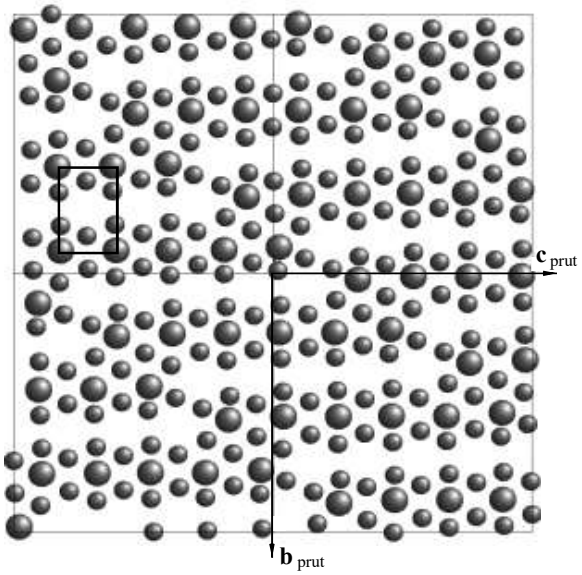

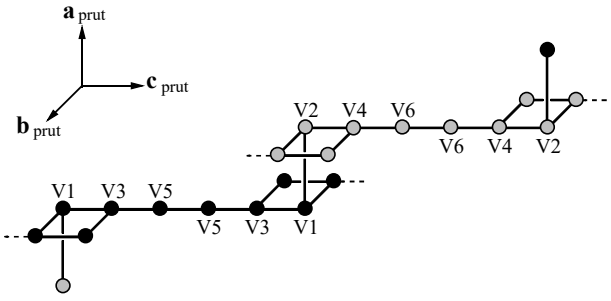

	V1-V2	V1-V3	V3-V5	V5-V5	V2-V4	V4-V6	V6-V6
298 K	2.77	2.95	2.91	2.80	2.95	2.85	2.82
20 K	2.77	2.90	2.99	2.79	3.06	2.62	3.30

Fig. 1 – Crystal structure of V_6O_{11}. Left: View along a_{prut}. Large and small circles mark vanadium and oxygen atoms, respectively. Right: V-chains V1-V3-V5-V5-V3-V1 (black circles) and V2-V4-V6-V6-V4-V2 (gray circles) belonging to adjacent vanadium layers. The table lists the measured V-V distances (Å) [15].

near the chain centers is the same as in the rutile structure. The projection of the latter is indicated by a rectangle. Our representation offers the great advantage of allowing reference of the single symmetry components of the V $3d$ orbitals to coordinate systems, which are common to the whole class of compounds. Inspired by previous work on the dioxides we will use local coordinate systems with the z- and x-axis parallel to the apical axis of the local octahedron and the pseudo-rutile c_{prut} axis, respectively [6–8].

The MIT of V_6O_{11} at 170 K is accompanied by a structural transformation, which preserves the triclinic space group $P\bar{1}$. Major changes concern the strong V4–V6 dimerization as well as ferroelectric-like shifts of atoms V3, V4, V5, and V6 away from the centers of the surrounding oxygen octahedra. In contrast, the V5–V5 dimerization and the strong ferroelectric-like shifts of atoms V1 and V2 are present in both phases with only minor changes. Hence, even with respect to the details of the local octahedral distortions, the chain centers and ends behave similarly to their parent structures VO_2 and V_2O_3.

The LDA calculations were performed using the scalar-relativistic augmented spherical wave (ASW) method [16] with a standard parametrization of the exchange-correlation potential [17]. Crystallographic data given by Canfield [15] were used. In order to account for the openness of the crystal structures, so-called empty spheres were included to model the correct shape of the crystal potential in large voids. Optimal empty sphere positions and radii of all spheres were determined automatically [18]. The basis set comprised V $4s$, $4p$, $3d$ and O $2s$, $2p$ as well as empty sphere states. Brillouin zone sampling was done using an increased number of $\boldsymbol{k}$ points ranging from 108 to 2048 points within the irreducible wedge.

Partial V $3d$ densities of states (DOS) resulting from calculations for the crystal structures of both phases are displayed in figs. 2 and 3. The gross features are very similar to those known from VO_2 and V_2O_3. Two groups of bands are identified, which result from crystal field splitting of the V $3d$ states due to the oxygen octahedra. Note that all orbitals are referred to the above local coordinate systems. While V $3d$ t_{2g} bands dominate in the energy region from -0.7 to 1.8 eV, the e_g states (not included in figs. 2 and 3) are found mainly between 2.0 and

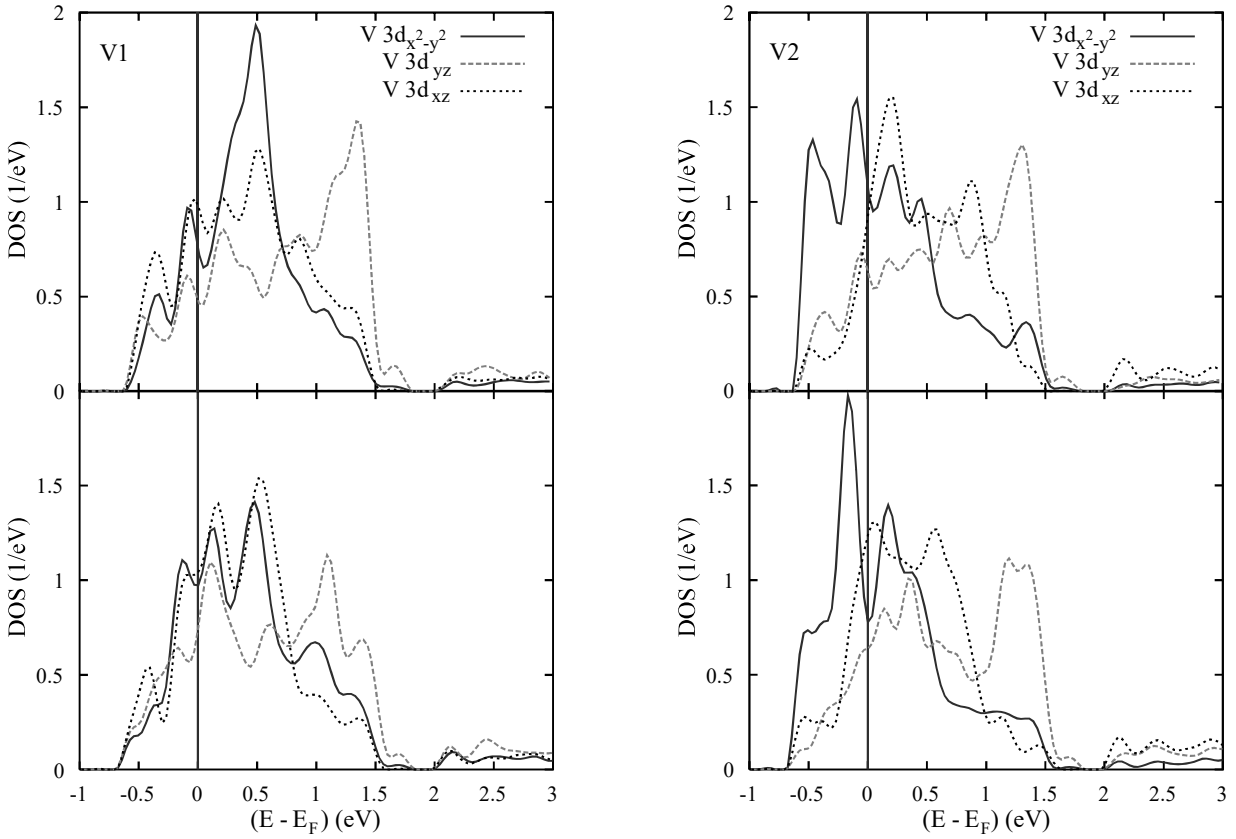

Fig. 2 – Partial V1 and V2 3*d* DOS (per atom) of high- (top) and low-temperature (bottom) V_6O_{11}.

4.8 eV. Small contributions from the t_{2g} states in this energy region result from distortions of the octahedra. Not shown are O 2*p* states occupying the energy region from −8.5 to −2.5 eV. Contributions of states in the energy range where the respective other orbital dominates are below 10%, but still indicative of covalent bonding. The electronic states obtained for the low-temperature phase miss the insulating gap, which is due to the well-known limitations of the LDA (and very similar to the situation reported for V_2O_3). However, these limitations are not important for the present work, as it aims primarily at the relation of the relevant orbitals to different local environments and their changes at the transition.

Going into more detail, we turn to the t_{2g} orbitals of those atoms which are involved in dioxide-like displacements, *i.e.* V4, V5, and V6. Their partial DOS are very similar among themselves and to those known from the rutile and monoclinic phase of VO_2 [6]. In particular, note the two-peak structure of the high-temperature V4 $d_{x^2-y^2}$ DOS, which is due to strong σ-type metal-metal bonding parallel to the vanadium chains (c_{prut}). In the low-temperature structure, V4–V6 dimerization causes increased splitting of this DOS into bonding and antibonding branches. At the same time, both the d_{yz} and d_{xz} partial DOS experience an energetical upshift due to increased *p*–*d* overlap arising from the ferroelectric displacement of the vanadium atom perpendicular to c_{prut}. As in VO_2, energetical separation between both types of bands is increased albeit not complete. The partial DOS of atom V5 display these features already in the metallic phase. In total, the partial DOS of the atoms V4, V5, and V6 can be fully understood in terms of the mechanisms known from VO_2.

The situation is different for the atoms V1 and V2, which are in a sesquioxide-like environment. In particular, they are involved in metal-metal bonding via shared octahedral faces

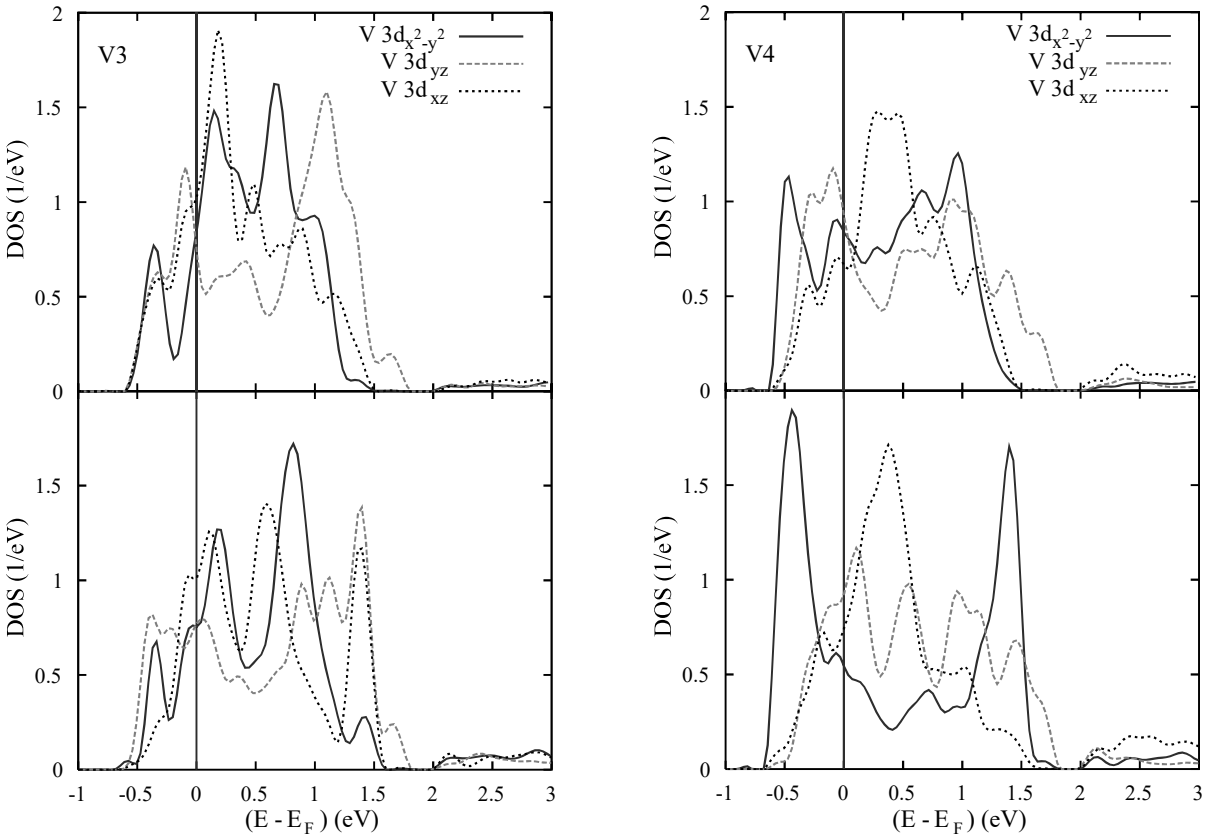

Fig. 3 – Partial V3 and V4 3*d* DOS (per atom) of high- (top) and low-temperature (bottom) V_6O_{11}.

across the layers. Furthermore, these atoms do not experience any dimerization. As a consequence, except for small peaks and shoulders near −0.5 and between 1.0 to 1.3 eV, which are reminiscent of the respective peaks of the chain center atoms, the $d_{x^2-y^2}$ DOS of atoms V1 and V2 consist of single rather broad peaks extending from −0.2 to 0.7 eV. In both phases, subpeaks observed in this energy region do not have counterparts in the DOS of neighbouring atoms indicative of metal-metal bonding. Like the d_{xz} states of these atoms, the $d_{x^2-y^2}$ states may thus be regarded as rather localized. This is in contrast to the d_{yz} states, which show bonding-antibonding splitting due to the aforementioned overlap across the layers, *i.e.* parallel to a_{prut}. Since this direction is parallel to the hexagonal c_{hex} axis of the corundum structure, the splitting of the d_{yz} states is equivalent to that of the a_{1g} states of V_2O_3. The partial DOS of atoms V1 and V2 thus can be interpreted in full accordance with the sesquioxide.

Atom V3 is exceptional since it does not fit into the above schemes: Neither does this atom experience dimerization along the chains as in VO_2, nor does it have neighbouring vanadium atoms across the layers as in V_2O_3. Yet, the partial DOS are rather similar to those of atoms V1 and V2. The $d_{x^2-y^2}$ and d_{xz} partial DOS form rather broad single peaks, the former still showing satellite peaks at −0.4 and 1.0/1.4 eV reminiscent of the bonding and antibonding peaks of atom V5. In contrast, the d_{yz} partial DOS displays a pronounced double-peak structure indicative of bonding-antibonding splitting. This puzzling situation is resolved by taking into account a different type of metal-metal bonding, namely that across octahedral faces along the sequences V1–V5–V3 and V2–V6–V4 parallel to b_{prut}. Hence, this σ-type overlap and the resulting bonding-antibonding splitting of the d_{yz} states is present not only for atom V3, but for all atoms. It is also observed in VO_2 [6]. For the d_{yz} states of atoms

V1 and V2 it adds to the above bonding parallel to a_{prut}; note that the respective antibonding peaks merge in the high-temperature phase. Although the coordination of atom V3 differs from that of all other atoms, its electronic properties are thus similar to that of the chain end atoms due to σ-type metal-metal overlap via octahedral faces within the layers. Hence, metal-metal bonding across the layers is not the only source of the splitting of the d_{yz} states.

In conclusion, while overlap of O $2p$ and V $3d$ states places the V $3d$ t_{2g} states near the Fermi energy, the detailed electronic properties of the latter and the MIT of V_6O_{11} are strongly influenced by the *local* metal-metal coordination. For this reason, the partial DOS for each atom may be regarded as local quantities. Near the chain centers (atoms V4 to V6) dimerization and ferroelectric-like displacements via strong electron-lattice interaction cause a splitting of the $d_{x^2-y^2}$ states and an energetical upshift of the d_{yz} and d_{xz} states. This is in complete analogy to the behaviour known from VO_2.

In contrast, near the chain ends (atoms V1, V2, and V3) the $d_{x^2-y^2}$ states experience less metal-metal overlap and, hence, become much more localized; their partial DOS resemble those of the d_{xz} states in the chain centers. As a consequence, electronic correlations might play a greater role. Being subject to metal-metal bonding only within the layers, the d_{yz} partial DOS of atom V3 displays bonding-antibonding splitting very similar to that of atoms V1 and V2. In addition, these atoms experience metal-metal overlap across the layers. We conclude that the V–V overlap within the layers is at least as important as the one perpendicular to them. In summary, the MIT of V_6O_{11} is interpreted as resulting from electron-lattice interaction and electronic correlations in the dioxide- and sesquioxide-like regions of the crystal, respectively.

Our findings have important implications for the understanding of V_2O_3. According to the above results, the electronic properties of this material are influenced by i) the localization of the $d_{x^2-y^2}$ states, and ii) the splitting of the d_{yz} states due to metal-metal bonding within layers perpendicular to the hexagonal c_{hex}-axis. Splitting of the a_{1g}-like states due to overlap parallel to c_{hex} might be less important than commonly assumed. Both effects could not be analysed in previous studies of V_2O_3 due to the high symmetry of this material. Yet, they are accessible to our present analysis of the sesquioxide-like regions of V_6O_{11}. Nevertheless, the electronic structure as well as the MIT of V_6O_{11} remain a crucial test case for all theories aiming at a correct description of both VO_2 and V_2O_3.

* * *

Fruitful discussions with S. Horn and S. Klimm are gratefully acknowledged. This work was supported by the Deutsche Forschungsgemeinschaft through SFB 484.

REFERENCES

[1] Goodenough J. B., *Prog. Solid State Chem.*, **5** (1971) 145.
[2] Brückner W., Oppermann H., Reichelt W., Terukow J. I., Tschudnowski F. A. and Wolf E., *Vanadiumoxide* (Akademie-Verlag, Berlin) 1983.
[3] Imada M., Fujimori A. and Tokura Y., *Rev. Mod. Phys.*, **70** (1998) 1039.
[4] Zylbersztejn A. and Mott N. F., *Phys. Rev. B*, **11** (1975) 4383.
[5] Wentzcovitch R. M., Schulz W. W. and Allen P. B., *Phys. Rev. Lett.*, **72** (1994) 3389.
[6] Eyert V., Habilitation Thesis, Universität Augsburg (1998); *Ann. Phys. (Leipzig)*, **11** (2002) 650.
[7] Eyert V., Horny R., Höck K.-H. and Horn S., *J. Phys. Condens. Matter*, **12** (2000) 4923.
[8] Eyert V., *Europhys. Lett.*, **58** (2002) 851.
[9] Pfalzer P., Will J., Nateprov A., Klemm M., Eyert V., Horn S., Frenkel A. I., Calvin S. and denBoer M. L., *Phys. Rev. B*, **66** (2002) 085119.

[10] Castellani C., Natoli C. R. and Ranninger J., *Phys. Rev. B*, **18** (1978) 4945; 4967; 5001.
[11] Held K., Keller G., Eyert V., Vollhardt D. and Anisimov V. I., *Phys. Rev. Lett.*, **86** (2001) 5345.
[12] Ezhov S. Yu., Anisimov V. I., Khomskii D. I. and Sawatzky G. A., *Phys. Rev. Lett.*, **83** (1999) 4136.
[13] Andersson S. and Jahnberg L., *Ark. Kemi*, **21** (1963) 413.
[14] Horiuchi H., Morimoto N. and Tokonami M., *J. Solid State Chem.*, **17** (1976) 407.
[15] Canfield P. C., PhD Thesis, University of California, Los Angeles (1990).
[16] Williams A. R., Kübler J. and Gelatt C. D. jr., *Phys. Rev. B*, **19** (1979) 6094; Eyert V., *Int. J. Quant. Chem.*, **77** (2000) 1007.
[17] Vosko S. H., Wilk L. and Nusair M., *Can. J. Phys.*, **58** (1980) 1200.
[18] Eyert V. and Höck K.-H., *Phys. Rev. B*, **57** (1998) 12727.